

Ultramultiple-level storage in TiN/SbTeN double-layer cell for high-density nonvolatile memory

You Yin,^{1,a)} Naoya Higano,² Hayato Sone,¹ and Sumio Hosaka¹

¹Department of Production Science and Technology, Gunma University, 1-5-1 Tenjin, Kiryu, Gunma 376-8515, Japan

²Department of Nano-Material Systems, Gunma University, 1-5-1 Tenjin, Kiryu, Gunma 376-8515, Japan

(Received 3 March 2008; accepted 8 April 2008; published online 25 April 2008)

We report a phase-change nonvolatile memory (NVM) concept based on a TiN/SbTeN (N-doped Sb₂Te₃) double-layer structure, which can be used for ultramultiple-level storage (UMLS). SbTeN shows a gradual resistivity drop and good phase stability with increasing annealing temperature, a characteristic which makes it suitable for UMLS applications. We demonstrate that the number of distinguishable resistance levels can readily reach 16 and even higher. These levels in this study result from the initial threshold switching and the subsequent current-controlled crystallization induced by Joule heating. The latter allows the creation of many distinct levels, thus, enabling the low-cost ultrahigh-density NVM. © 2008 American Institute of Physics. [DOI: 10.1063/1.2917471]

There is a rapidly increasing demand for ultrahigh-density nonvolatile memory (NVM) due to today's explosive proliferation of information. This type of memory can stably store information even if no power is supplied.¹⁻⁷ An extremely attractive characteristic of the future's NVM is multiple-level storage (MLS), which is data storage on more than two levels per memory cell; it makes a dramatic increase in memory capacity possible, i.e., much more information can be saved without increasing the cell size. This leads to a decrease in the cost per bit.

Among the emerging NVMs which are expected to replace the current nonvolatile flash memory, both phase-change memory (PCM) with stacked chalcogenide layers⁸⁻¹⁰ and resistive random access memory^{11,12} (RRAM) have been shown to have MLS potential for future ultrahigh-density memory. However, the number of storage levels strongly depends on the number of chalcogenide layers and only a four-level storage was demonstrated up until now due to the difficulty in design.⁸ Moreover, the fact that the mechanism of RRAM is yet unclear^{11,13} might severely hinder the deep study of its MLS potential. It is well known that PCM is based on a resistivity difference of up to around three orders of magnitude caused by the structural transition between the amorphous and the crystalline phases. Therefore, in theory, PCM is very suitable for ultramultiple-level storage (UMLS, e.g., over eight levels) due to the great number of possible intermediate resistance states between the two phases which can be produced by controlling the total crystallinity between the electrodes. Practically, however, most current vertical PCMs with an in-series heater exhibit sharp resistance changes with the programming pulse amplitude, which makes them very difficult to apply to UMLS in a stable and controllable way.¹⁴⁻¹⁹

Here, we report a lateral double-layer structure using TiN/SbTeN (N-doped Sb₂Te₃), whose total crystallinity of the phase-change material between the electrodes can be very precisely controlled with the help of the top TiN layer. This controllability is realized mainly through the gradual

enlargement of the crystalline zone induced by current-driven Joule heating.

200-nm-thick SbTeN film samples with a SiO₂ capping layer on glass substrates were prepared by simultaneously introducing both N₂ and Ar into the chamber using a radio frequency sputtering equipment (MNS-3000-RF, ULVAC, Inc.) at a background pressure below 5×10^{-5} Pa and a sputtering pressure of 0.2 Pa. SbTe and SbTeN films were prepared at N₂/Ar flow ratios of 0/15 and 1/14 [SCCM/SCCM (SCCM denotes cubic centimeter per minute at STP)], respectively. The nitrogen concentration was determined to be 1.63% in SbTeN films by x-ray photoelectron spectroscopy (Perkin Elmer ESCA5600). Crystal structures of films of each kind were characterized by x-ray diffractometer (RINT 2000, Rigaku Co.) after annealed on a hot plate from 90 to 290 °C for 5 min. Resistivity as a function of annealing temperature of films was measured by using square-shaped film samples (12 × 12 mm²) defined by Ti electrodes. Current-voltage (*I-V*) characteristics of the device samples were measured by semiconductor parameter analyzer (4155B, Agilent Technologies, Ltd.).

Figure 1(a) shows the crystal structure and resistivity as functions of the annealing temperature up to 300 °C based

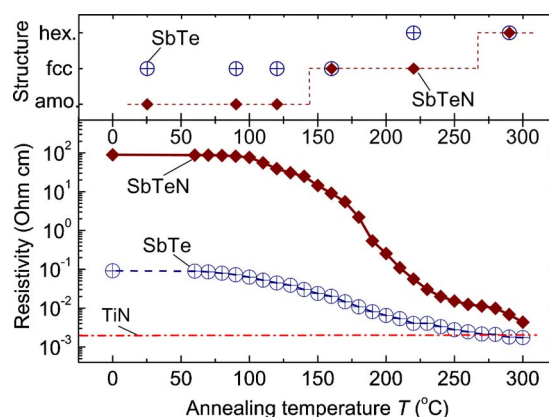


FIG. 1. (Color online) Crystal-structural change and resistivity as functions of increasing annealing temperature of N-doped Sb₂Te₃ (SbTeN) and Sb₂Te₃ (SbTe) and TiN films.

^{a)}Electronic mail: yinyou@el.gunma-u.ac.jp.

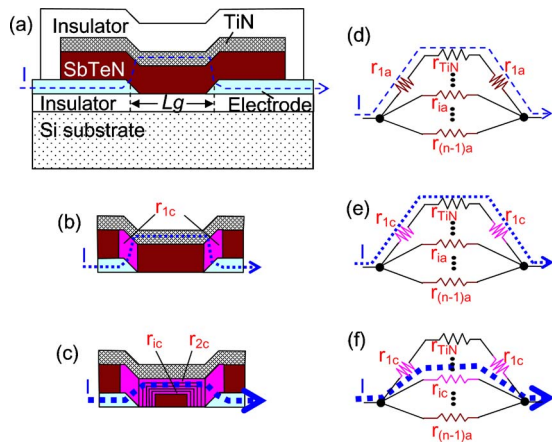


FIG. 2. (Color online) Principle of UMLS in the TiN/SbTeN double-layer structure. (a) Schematic cross-sectional diagram of the device when SbTeN is wholly amorphous. (b) Crystallization at the two steps induced by the current $I (> I_{th})$. (c) Enlargement of the crystalline zone with increasing current. [(d)–(f)] Equivalent circuits of the resistance states of the device corresponding to [(a)–(c)], respectively.

on x-ray diffraction patterns and the electrical measurement of the films. The SbTe film was found to have a face-centered cubic (fcc) crystal structure below around 180 °C. It changes to a hexagonal (hex) crystal structure as the annealing temperature increases further. However, the N doping of SbTe clearly increases the temperatures of the structural transitions from the amorphous (amo) structure to fcc and then to hex. The two temperatures are around 140 and 270 °C, respectively. The resistivity of as-deposited SbTe film was as low as $\sim 9 \times 10^{-2} \Omega \text{ cm}$ because as-deposited SbTe film is already fcc crystalline. The resistivity of SbTe film decreased within the temperature range of 100–300 °C. This reduction in resistivity was due to the phase transformation from fcc to hex. In contrast, the resistivity of as-deposited amorphous SbTeN film was 1000 times that of SbTe film. Crystallization to fcc led to a marked reduction in resistivity from around 9×10^1 to around $8 \times 10^{-3} \Omega \text{ cm}$, a difference of about four orders of magnitude. The phase transformation from fcc to hex resulted in a further resistivity drop to around $4 \times 10^{-3} \Omega \text{ cm}$ at 300 °C. TiN films have a resistivity of around $2 \times 10^{-3} \Omega \text{ cm}$. The N doping into chalcogenides retards the growth of crystals and refines the crystals in the films. The gradual decrease in resistivity of the SbTeN films with increasing temperature should be due to the gradual growth of crystals, i.e., the gradual change in crystal structure.^{19,20} The threshold field E_{th} of SbTeN was determined to be 14.3 V/ μm , which is close to the value for doped SbTe reported by Lonkhorst *et al.*²¹

Figure 2 shows our concept of UMLS (e.g., n resistance levels here) based on the filament formation, crystallization, and subsequent enlargement of the crystalline zone. Figure 2(a) shows a schematic cross-sectional diagram of a device with a TiN/SbTeN double layer. It is well known that phase-change materials exhibit threshold switching.^{21,22} Such switching occurs due to the formation of conductive filaments and crystallization when the electric field over the amorphous volume exceeds the threshold field E_{th} . By applying a current I_1 above I_{th} (corresponding to the electric field E_{th}), the concentration of the electric field induces local crystallization at the steps of the SbTeN layer [pink areas in Fig. 2(b)] according to our previous simulation.⁹ The crystalliza-

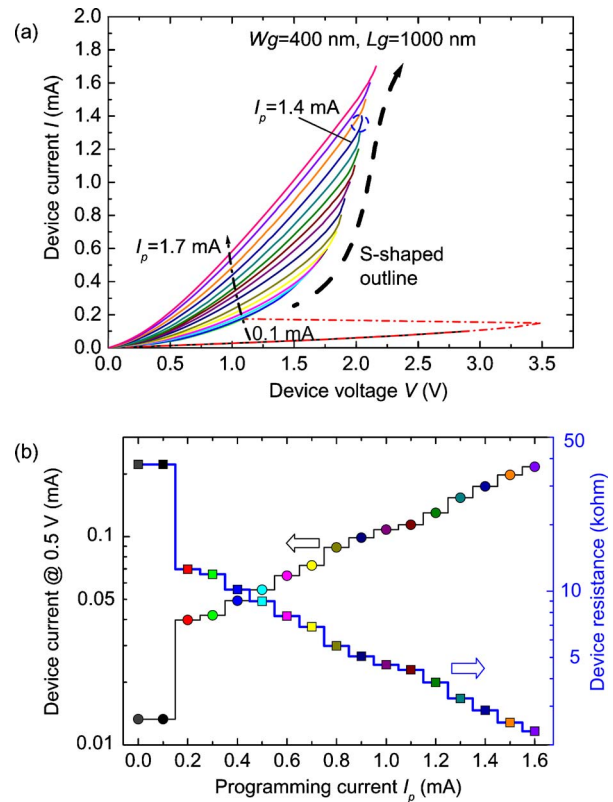


FIG. 3. (Color online) UMLS in the TiN/SbTeN double-layer device. SbTeN and TiN layers are 150 and 50 nm in thickness, respectively. (a) I - V curves when current sweeping from 0 mA to the programming current I_p . I_p increases from 0.1 to 1.7 mA in 0.1 mA increments. (b) Device current at 0.5 V and resistance as functions of the programming current.

tion makes the resistances at the steps of the SbTeN layer drop from r_{1a} to r_{1c} [see Figs. 2(d) and 2(e)]. Therefore, the total device resistance drops from R_0 to R_1 . R_0 and R_1 correspond to Figs. 2(a) [or 2(d)] and 2(b) [or 2(e)], respectively. Furthermore, the crystalline zone is expected to gradually expand with the increasing current by Joule heating from the top of the SbTeN layer between the electrodes. The first crystallization enlargement by applying a current I_2 happens at the region marked by r_{2c} , as shown in Fig. 2(c). The device resistance correspondingly drops from R_1 to R_2 . Similarly, the $(i-1)^{th}$ enlargement of the crystalline zone is triggered by applying I_i . The resistance change from r_{ia} to r_{ic} results in a drop of the total device resistance from R_{i-1} to R_i . As we can see from above description, the TiN layer plays an important role when programming the device. The current path between electrodes is changed to that via the top TiN layer shown in Fig. 2(a) and facilitates the electric field concentration. The subsequent Joule heating from the TiN layer makes it possible to realize the gradual enlargement of the crystalline zone.

Figure 3(a) shows the current-voltage (I - V) curves when current sweeping with increasing maximum current (programming current I_p), which is in the range of 0.1–1.7 mA. Current sweeping from 0 to 0.1 mA, shown as the black dotted curve, did not change the resistance level at all, and the SbTeN layer remained completely amorphous (Curve $I_p=0.1$). Current sweeping up to 0.2 mA, shown as the red dash dotted curve, i.e., above the threshold current (around 0.15 mA), induced sudden switching (Curve $I_p=0.2$ mA). The switching should be due to the crystallization process at

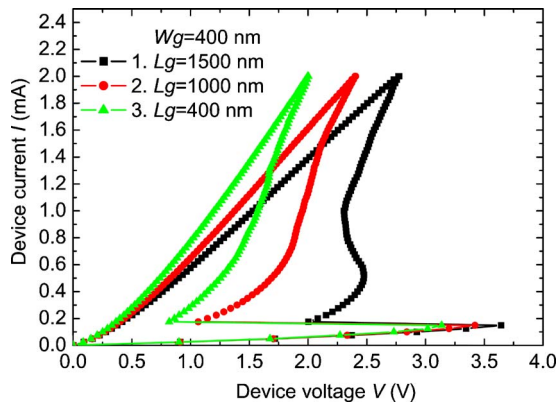


FIG. 4. (Color online) I - V curves of devices with different sizes.

the steps [corresponding to the change from Fig. 2(a) to Fig. 2(b)]. It is clearly seen from the subsequent curves that two regions (the retaining and programming regions) were created when current sweeping with even higher programming current. For Curve $I_p = 1.4$ mA, for example, the resistance switching process could be clearly observed between 1.3 and 1.4 mA (inside the dashed blue circle), while the resistance level programmed at 1.3 mA could be retained up to the previous programming current (1.3 mA). It is very interesting that the switching outline of the curves is generally S shaped and continuous (dashed black arrow). The programmed resistance could be read out at a certain current or voltage. Figure 3(b) shows the current at 0.5 V and the calculated resistance as functions of the programming current. The first sudden resistance drop due to threshold switching was caused by the crystallization at the steps in the SbTeN layer shown in Fig. 2(b). The subsequent gradual resistance drops resulted from the enlargement of the crystalline zone shown in Fig. 2(c). Sixteen distinct resistance levels were created in this study, and they were induced by current-driven programming. The test devices with the same size exhibited good uniformity when the initial resistance levels were the same. It should be noted that low currents were used for the programming device, despite the very large size of the device (the gap length L_g was 1000 nm and the gap width W_g was 400 nm).

The dependence of the gap length on the I - V curves is shown in Fig. 4. All of the threshold currents are around 0.15 mA. The threshold current I_{th} can be expressed as $I_{th} = E_{th}thc/r_{1a}$, where th is the thickness of the SbTeN layer and c is the thickness ratio at the step and blanket regions. Here, c was estimated to be 0.7–0.8. As a result, a difference in gap length would not lead to a difference in threshold current for devices with the same parameters except the gap length. The threshold voltage of the device should be slightly dependent on the gap length due to the partial voltage drop in the top TiN layer and the gap-length dependence of the resistance of the TiN layer. The S-shaped switching outline can be more clearly observed when the gap is longer. Thus, in-

creasing the gap length might facilitate UMLS with a good uniformity or an increased window margin. If we assume that the phase transformation of the volume V_1 caused by the first crystallization process during the threshold switching, as shown in Fig. 2(b), and the total programmable volume including the subsequent crystallization processes is V_{total} , the volume $V_{total} - V_1$ programmed by the subsequent Joule heating increases with the gap length. This increase might result in the above-mentioned gap-length dependence of the I - V curves.

In summary, we demonstrated UMLS based on low-power crystallization instead of high-power amorphization by using a TiN/SbTeN double-layer PCM cell structure. The crystallization induced by Joule heating is nonvolatile, low-power, and current-driven, and allows UMLS. This phenomenon can be employed in practical applications to dramatically increase the memory capacity without increasing the cell size.

The authors would like to express their gratitude for the financial support by the Semiconductor Technology Academic Research Center (STARC) of Japan.

- ¹S. R. Ovshinsky, *Phys. Rev. Lett.* **21**, 1450 (1968).
- ²A. Beck, J. G. Bednorz, Ch. Gerber, C. Rossel, and D. Widmer, *Appl. Phys. Lett.* **77**, 139 (2000).
- ³L. Guo, E. Leobandung, and S. Y. Chou, *Science* **275**, 649 (1997).
- ⁴J. Ouyang, C.-W. Chu, C. R. Szmanda, L. Ma, and Y. Yang, *Nat. Mater.* **3**, 918 (2004).
- ⁵K. Terabe, T. Hasegawa, T. Nakayama, and M. Aono, *Nature (London)* **433**, 47 (2005).
- ⁶Y. Yin, H. Sone, and S. Hosaka, *Jpn. J. Appl. Phys., Part 1* **45**, 4951 (2006).
- ⁷R. Pandian, B. J. Kooi, G. Palasantzas, J. T. M. D. Hosson, and A. Pauza, *Appl. Phys. Lett.* **91**, 152103 (2007).
- ⁸J. Feng, Y. F. Lai, B. W. Qiao, B. C. Cai, Y. Y. Lin, T. A. Tang, and B. Chen, *Jpn. J. Appl. Phys., Part 1* **46**, 5724 (2007).
- ⁹Y. Yin, H. Sone, and S. Hosaka, *Microelectron. Eng.* **84**, 2901 (2007).
- ¹⁰F. Rao, Z. Song, M. Zhong, L. Wu, G. Feng, B. Liu, S. Feng, and B. Chen, *Jpn. J. Appl. Phys., Part 2* **46**, L25 (2007).
- ¹¹M. J. Rozenberg, I. H. Inoue, and M. J. Sanchez, *Phys. Rev. Lett.* **92**, 178302 (2004).
- ¹²Y. Watanabe, J. G. Bednorz, A. Bietsch, Ch. Gerber, D. Widmer, A. Beck, and S. J. Wind, *Appl. Phys. Lett.* **78**, 3738 (2001).
- ¹³S. T. Hsu, T. Li, and N. Awaya, *J. Appl. Phys.* **101**, 024517 (2007).
- ¹⁴Y. Yin, H. Sone, and S. Hosaka, *Jpn. J. Appl. Phys., Part 1* **45**, 6177 (2006).
- ¹⁵S. Lai and T. Lowrey, *Tech. Dig. - Int. Electron Devices Meet.* **2001**, 803.
- ¹⁶A. L. Lacaíta, *Solid-State Electron.* **50**, 24 (2006).
- ¹⁷S. Hosaka, K. Miyauchi, T. Tumura, Y. Yin, and H. Sone, *IEEE Trans. Electron Devices* **54**, 517 (2007).
- ¹⁸B. Liu, Z. Song, S. Feng, and B. Chen, *Microelectron. Eng.* **82**, 168 (2005).
- ¹⁹Y. Yin, H. Sone, and S. Hosaka, *J. Appl. Phys.* **102**, 064503 (2007).
- ²⁰Y. Yin, H. Sone, and S. Hosaka, *Jpn. J. Appl. Phys., Part 1* **45**, 8600 (2006).
- ²¹M. H. R. Lankhorst, B. W. S. M. M. Ketelaars, and R. A. M. Wolters, *Nat. Mater.* **4**, 347 (2005).
- ²²S. R. Ovshinsky and H. Fritzsche, *IEEE Trans. Electron Devices* **ED-20**, 91 (1973).